

Figure 1 Schematic representation of one cycle of the collision model, in which particles that collide when sheared are given small random displacements.

Each shear cycle is decomposed into three steps: (i) determine particle positions (black dots); (ii) shear the system by a strain amplitude γ_0 and find particle pairs that collide (that is, come within a distance d of each other, indicated by overlapping red circles of diameter d); (iii) reset the initial positions and randomly displace particles that collided (dashed red circles \rightarrow blue circles). For each shear cycle, particles are displaced as many times as they collide. The chance of particles colliding increases with the strain amplitude γ_0 and volume fraction ϕ .

are self-organized to avoid collisions, resulting from a process of ‘random organization’.

To gain some intuition, we first describe a one-dimensional version of our model. To start, N point particles are randomly distributed along a line of length L . Next, one of the particles is displaced a distance l along the line, possibly encountering other particles, and then returned to its initial position. For each encounter, both the displaced particle and the one it encounters are given random displacements of maximum amplitude ϵ from their initial positions, which can increase or decrease the distance Δx between them. This process is repeated cyclically for all the particles.

According to these rules, particles in regions where $\Delta x \leq l$ receive random displacements and are active, and thus undergo diffusive motion. In regions with $\Delta x > l$, particles do not encounter each other and are inactive, with particles returning after each cycle to their initial positions. Active regions can activate neighbouring inactive regions and the process can continue forever, provided there is always some region where $\Delta x \leq l$ (see Supplementary Information, video S1). However, if a configuration develops where $\Delta x > l$ for all neighbouring particle pairs, there are no more displacements and dynamics cease (see Supplementary Information, video S2). The system has reached an absorbing state.

It is clear that at $l = L/N$, the inverse density, there is a unique absorbing state: all particles are equidistant with $\Delta x = L/N$. For $l > L/N$, there are no absorbing states; motion can never cease and particles diffuse. For $l < L/N$, there is an infinite number of absorbing states. Our simulations show that there is a phase transition at a critical value $l_c \simeq 0.91 \pm 0.01L/N$ characterized by an order parameter, the steady-state fraction of active particles f_a^∞ , which for $l \rightarrow l_c^+$ scales as $f_a^\infty \sim [(l - l_c)/l_c]^\beta$ with $\beta \simeq 0.42 \pm 0.10$. Thus, there exist absorbing states for $l > l_c$ that are not found.

For $l < l_c$ the system finds an absorbing state in a finite time $t = \tau$ (number of cycles). For $l \rightarrow l_c^-$ the relaxation time τ diverges as $\tau \sim [(l_c - l)/l_c]^{-\nu}$ with $\nu \simeq 2.48 \pm 0.10$, and is independent of the system size for large systems. For $l > l_c$ the time to establish a steady state likewise shows power-law behaviour, $\tau \sim [(l - l_c)/l_c]^{-\nu}$. Unlike the ‘protein-folding problem’, where the time to search for a unique folded state by a random walk diverges as the size increases²¹, here the time to find one of the infinite number of absorbing states is finite. The exponents β and ν , which characterize the asymptotic critical behaviour of the order parameter f_a^∞ and the relaxation time τ , do not correspond to those found for DP ($\beta_{DP} \simeq 0.276$ and $\nu_{DP} \simeq 1.73$); therefore, our model does not belong to the DP

Figure 2 Simulation results for the 2D model, showing particle activity above and below the strain threshold. **a,b**, Snapshots of the particle distributions for two strain amplitudes $\gamma_0 = 3.0$ and 2.0 , area fraction $\phi = 0.2$ and 1,000 particles. The number of shear cycles that have passed is indicated below each snapshot. Filled black circles indicate particles that will collide and thus be irreversibly displaced in the next shear cycle; open circles indicate particles whose trajectories are reversible. The shear flow direction is horizontal. **c**, Fraction of active particles per cycle f_a as a function of number of shear cycles for the two different strain amplitudes shown in **a** and **b**: $\gamma_0 = 3.0$ (red) and $\gamma_0 = 2.0$ (blue). Full lines show fits to equation (1). Inset: Fraction of active particles in steady state as a function of strain amplitude γ_0 . The full line in the inset shows the scaling $f_a^\infty \sim |\gamma_0 - \gamma_0^c|^\beta$ where $\beta = 0.45 \pm 0.02$, obtained by a fit to the data. The blue and red data points indicate the data below ($f_a^\infty = 0$) and above ($f_a^\infty > 0$) the critical strain amplitude γ_0^c .

universality class, as expected, because the number of particles is conserved in our model whereas in DP it is not^{22,23}.

A 2D version of the model mimics a suspension of particles subjected to periodic shear, as illustrated in Fig. 1. First, $N = 1,000$ discs are randomly distributed in a two-dimensional rectangular box. The interaction distance d sets the unit of length and the area of the box A is chosen to obtain the desired area (2D volume) fraction $\phi = N\pi d^2/4A$. The system is sheared with a strain amplitude γ_0 , which causes some particles to encounter each other, as illustrated in Fig. 1. As in the one-dimensional case, particles that collide are given a random displacement from their initial position. The net displacement of a particle after one cycle is zero if it does not encounter any other particle. The direction of the random displacements is uniformly distributed in the plane and their amplitude is uniformly distributed between zero and a maximum value ϵ , typically a fraction of a particle diameter d .

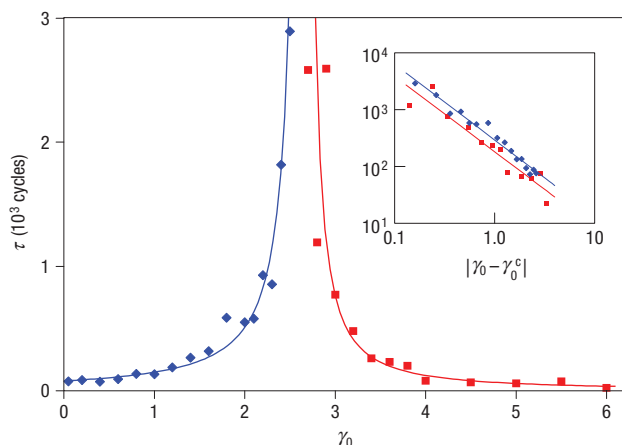


Figure 3 Simulation results for the characteristic time τ to reach steady state as a function of the strain amplitude γ_0 for an area fraction of $\phi = 0.20$ and 1,000 particles. Blue symbols, below transition ($\gamma_0 < \gamma_0^c$); red symbols, above transition ($\gamma_0 > \gamma_0^c$). Full lines show the power-law fits: $\tau \sim |\gamma_0 - \gamma_0^c|^{-\nu}$ with $\nu = 1.33 \pm 0.02$. Inset: The same data and fit plotted as a function of $|\gamma_0 - \gamma_0^c|$ on a log-log scale with $\gamma_0^c = 2.66 \pm 0.05$.

The results are insensitive to the precise value of ϵ provided that it is not too large compared to d . In the following, $\epsilon = d/2$. An aspect ratio of 2 is arbitrarily chosen for the box and shear is applied along the longer dimension using periodic boundary conditions. Other simulations using various population sizes, box aspect ratios, boundary conditions and three-dimensional systems were also tried. All lead to the same qualitative results as those reported here.

Figure 2 shows the behaviour of two particle populations subjected to strain amplitudes $\gamma_0 = 3$ and 2 for an area fraction $\phi = 0.20$. The two series of snapshots shown in Fig. 2a and b illustrate the evolution of particle distributions as a function of the number of shear cycles for each γ_0 . Because the initial particle distributions are random, the first few cycles generate many collisions for both γ_0 . After a few hundred cycles, however, two distinct behaviours emerge. For $\gamma_0 = 2$, the fraction f_a of active particles per cycle decreases and eventually vanishes (Fig. 2c and Supplementary Information, video S3). At this point, the particle distribution corresponds to the last snapshot in Fig. 2b. All the particles have found a position such that they no longer collide with each other when the system is sheared. By contrast, for $\gamma_0 = 3$, the system reaches a steady state where a finite fraction of particles always collide with another particle. In this case, f_a decreases towards a non-zero steady-state value f_a^∞ , about which it fluctuates indefinitely (Fig. 2c and Supplementary Information, video S4).

The relaxation curves shown in Fig. 2c are well fitted by the following form:

$$f_a(t) = (f_a^0 - f_a^\infty) \frac{e^{-t/\tau}}{t^\delta} + f_a^\infty, \quad (1)$$

where f_a^0 and f_a^∞ are, respectively, the initial and steady-state values of f_a . The fit to equation (1) shows that the relaxation data $f_a(t)$ exhibits the usual crossover from exponential to power-law behaviour that one expects for critical phase transitions.

The inset in Fig. 2c shows how the steady-state value f_a^∞ varies with strain amplitude γ_0 . A clear transition from absorbing states ($f_a^\infty = 0$) to fluctuating diffusive states ($f_a^\infty > 0$) is visible at a critical strain amplitude of $\gamma_0^c = 2.66 \pm 0.05$. The steady-state

active fraction f_a^∞ serves as an order parameter and can be fitted asymptotically above the transition to $f_a^\infty \sim (\gamma_0 - \gamma_0^c)^\beta$ with $\beta = 0.45 \pm 0.02$. These data can be recast in terms of a diffusion coefficient D defined by $D = \langle \delta r_1^2 \rangle / 2$, where $\langle \delta r_1^2 \rangle$ is the mean square displacement per cycle averaged over all the particles. Close to γ_0^c , a behaviour similar to that for f_a^∞ is obtained: $D \sim (\gamma_0 - \gamma_0^c)^\beta$.

The characteristic time τ for the system to reach steady state, obtained from the fit to equation (1), diverges at the same critical strain amplitude $\gamma_0^c \simeq 2.66$, as shown in Fig. 3. For $\phi = 0.20$, this divergence follows a power law given by $\tau \sim |\gamma_0 - \gamma_0^c|^{-\nu}$ with $\nu = 1.33 \pm 0.02$.

As in the one-dimensional case, there exist absorbing states in two (and three) dimensions above the threshold that the system does not find. For example the threshold in the 2D simulations is $\gamma_0^c \simeq 2.66$ for $\phi = 0.2$. If we arrange the spheres in parallel rows with each almost touching horizontally, and stack the rows so that the spheres are on top of each other from one row to the next (that is, a square lattice), then we can fill space to $\phi = \pi/4 \simeq 0.789$ and shear the system without limit to any amplitude with no collisions. Thus the square lattice is an absorbing state for any strain as long as $\phi < \pi/4$. Similarly, in three dimensions we have an absorbing state of sliding hexagonal planes of spheres for any $\phi < 0.734$. This demonstrates that, in spite of the fact that there are absorbing states for $\phi > \phi_c$, not all absorbing states are found. Moreover, if we create such an absorbing state and apply a strain amplitude $\gamma > \gamma_0^c$, we find that it is unstable: given a perturbation, particles start colliding and the disturbance grows until the system arrives at the same dynamic diffusive state (same order parameter) as if started from the random state.

In spite of its simplicity, the model exhibits a threshold similar to the one observed in the experiments concerning the onset of irreversibility in non-brownian suspensions¹⁷. In these experiments, particles suspended in a viscous fluid exhibited diffusion when the strain amplitude γ_0 of the oscillatory shear was above some concentration-dependent critical value γ_0^c but simply oscillated back and forth without diffusion when γ_0 was below γ_0^c .

More importantly, the model shows that the absence of particle diffusion below the threshold occurs because the particles are able to self-organize into a configuration where they no longer collide; that is, they adopt configurations such that they no longer approach close enough to each other to interact irreversibly. Above the threshold, particles also develop some correlations, but these are insufficient to avoid collisions, consistent with studies of non-oscillatory steady shear flow²⁴. Thus, a key prediction of our model is that below the threshold strain amplitude γ_0^c there should be a transient during which the system organizes itself from a diffusing active state to an organized absorbing state. To test this prediction, we set up the same oscillatory Couette system as in¹⁷, but devised several means to follow the transient behaviour when the system was prepared in a more-or-less random state (see the Methods section).

The experimental system consists of (230 ± 20) - μm -diameter plastic particles suspended in a viscous liquid that is density and index matched to the particles. Suspensions are placed between concentric cylinders in a Couette cell. The inner cylinder is rotated about its axis back and forth through a small angle $\Delta\theta$ to produce an oscillatory time-dependent strain of $\gamma(t) = \gamma_0 \sin(2\pi t/T)$, where γ_0 is the strain amplitude and T is the period at which the inner cylinder is rotated back and forth. The radius a of the inner cylinder is 25 mm and the gap g between the inner and outer cylinders is 2.5 mm. Thus the strain amplitude is $\gamma_0 = a \Delta\theta/g$. The period T is held fixed at 25 s for the whole range of strain amplitudes considered: $0.6 \leq \gamma_0 \leq 2.5$. The Reynolds number, as estimated from the gap, fluid viscosity and maximum velocity, is kept less than 10^{-3} , where pure fluids are reversible.

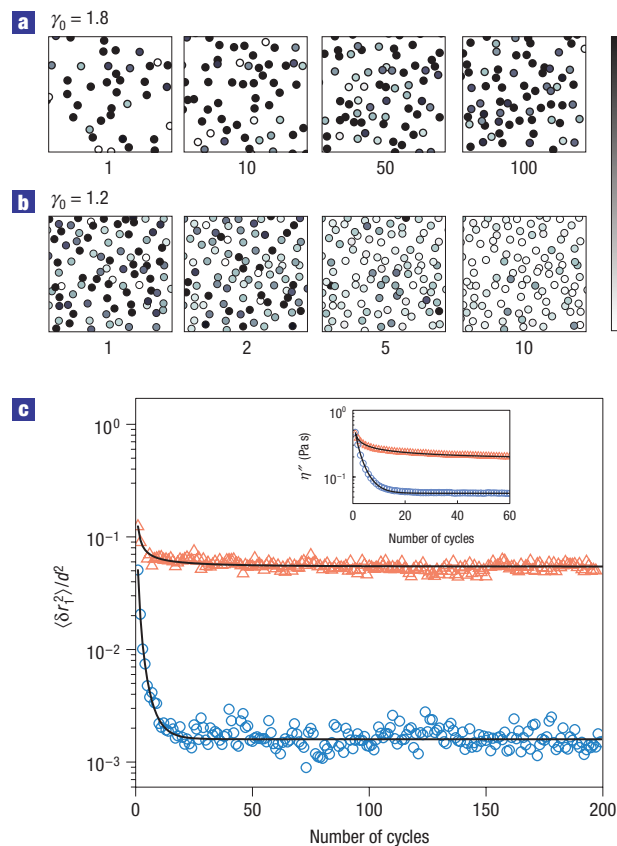


Figure 4 Experimental results showing particle activity above and below the strain threshold. **a,b**, Snapshots of the particle distributions for two strain amplitudes $\gamma_0 = 1.8$ and 1.2 ; volume fraction $\phi = 0.3$. Particles within a plane are visualized by passing a laser sheet through a Couette cell: the horizontal and vertical axes are the shear and vorticity directions. The grey scale and associated numbers indicate the amplitudes of particle displacements in micrometres in the previous shear cycle. **c**, Mean square displacement per cycle $\langle \delta r_1^2 \rangle$ as a function of the number of cycles for the strain amplitudes shown in **a** and **b**: $\gamma_0 = 1.8$ (red) and $\gamma_0 = 1.2$ (blue). Inset: The in-phase response of the complex viscosity η'' as a function of the number of cycles: $\gamma_0 = 1.8$ (red) and $\gamma_0 = 1.2$ (blue). The lines show fits to equation (1).

To follow the motion of the suspended particles, fluorescent dye (Rhodamine 6G) is added to visualize the index-matched particles. The particles in a given plane can be imaged by exciting the dye with a sheet of laser light 200–300 μm thick. Within the thickness of this laser sheet, the fluid fluoresces while particles appear as dark spots. This approach allows us to simultaneously follow the motion of many particles (see Supplementary Information, video S5) and obtain the statistics required to investigate the transient regimes.

Results are presented in Figs 4 and 5 for a volume fraction of $\phi = 0.30$. Figure 4a,b shows the evolution of particle positions as a series of snapshots for two strain amplitudes $\gamma_0 = 1.8$ and 1.2 , respectively. Tracked particles are represented with circles having the same diameter as the particles. The shading of each circle depends on the magnitude of the particle displacement from the previous shear cycle. For both strain amplitudes, the first cycles generate many rearrangements with large irreversible displacements of more than 40 μm , or 20% of a particle diameter. Consistent with the model, the size and number of these displacements quickly decreases for the lower strain amplitude of $\gamma_0 = 1.2$. Despite a few local rearrangements, particles return

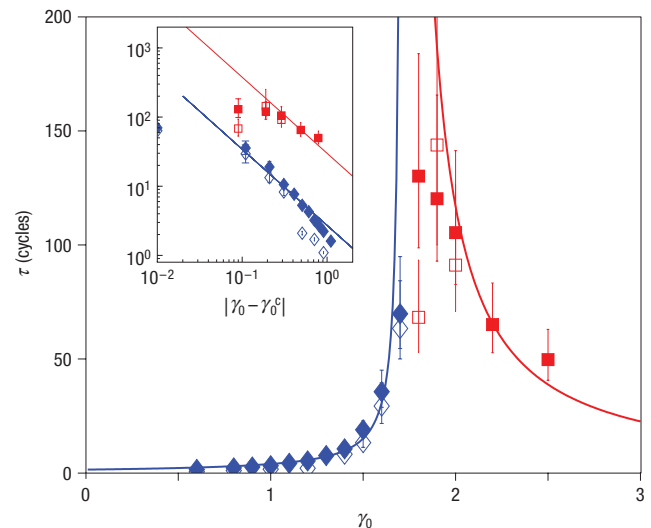


Figure 5 Experimental results for the characteristic time τ to reach steady state as a function of the strain amplitude γ_0 for a volume fraction $\phi = 0.30$. Open symbols, $\langle \delta r_1^2 \rangle$ data; solid symbols, η'' data; blue symbols, below transition ($\gamma_0 < \gamma_0^c$); red symbols, above transition ($\gamma_0 > \gamma_0^c$). Full blue lines show a power-law fit to the data below the transition: $\tau \sim |\gamma_0 - \gamma_0^c|^{-\nu}$ with $\nu = 1.1 \pm 0.3$ and $\gamma_0^c = 1.71 \pm 0.15$. Full red lines show the same power law found below the transition for comparison as there are too few data points to extract a reliable exponent. Inset: Same data and fit plotted as a function of $|\gamma_0 - \gamma_0^c|$ on a log–log scale.

to their starting positions to within less than 5 μm (Fig. 4b and Supplementary Information, video S6). The suspension finds a reversible, absorbing state. By contrast, for larger strain amplitudes, clusters of particles are constantly displaced (Fig. 4a and Supplementary Information, video S7) and diffusion results.

The dynamics of the self-organization process and the degree of irreversibility can be characterized using the mean square displacement per cycle $\langle \delta r_1^2 \rangle$ in the plane of the laser sheet. Figure 4c shows that there is a transient in $\langle \delta r_1^2 \rangle$, which starts out large and then monotonically decreases until it reaches a steady-state value.

We detect the same transient behaviour in the stress response of the suspension. For this, a rheometer measures the time-dependent stress required to make the inner cylinder oscillate. From this signal, we extract the component of stress σ' that is in phase with the shear strain $\gamma(t)$ and the corresponding in-phase viscosity, usually denoted η'' and defined as $\eta'' = \sigma' / \dot{\gamma}_0$, where $\dot{\gamma}_0 = 2\pi\gamma_0/T$ is the amplitude of the strain rate. The inset of Fig. 4c shows the transient observed for η'' as a function of the number of cycles. Even though the relationship between irreversible motion and rheological response is not completely clear, this rheological signature is a convenient measure of the time-dependent system dynamics. In contrast to the image analysis technique used to measure f_a , rheological measurements average over the entire suspension, and thus sample many more particles, which yields a much greater signal-to-noise ratio.

Figures 4 and 5 demonstrate that the same phase transition is observed in the real system as in the model. The data for both $\langle \delta r_1^2 \rangle$ and η'' are well fitted to equation (1), as shown in Fig. 4. A sharp transition from absorbing reversible states to diffusive states occurs at a critical strain amplitude of $\gamma_0^c = 1.71 \pm 0.15$ for $\phi = 0.30$. Above γ_0^c , the steady-state value of $\langle \delta r_1^2 \rangle$ varies as $(\gamma_0 - \gamma_0^c)^\beta$ with $\beta = 0.45 \pm 0.10$. The characteristic time τ to reach the steady state also diverges at the same critical strain amplitude γ_0^c , as shown in Fig. 5. This divergence follows a power law with exponent

$\nu = 1.1 \pm 0.3$. Although the values of the critical exponents are not expected to be the same in the simplified 2D model and the 3D experiments, the basic structure of the divergences is nearly identical. Furthermore, the collision-induced self-organization must be responsible for the small Lyapunov exponent found numerically below threshold using Stokesian dynamics¹⁷. In this case, the source of irreversibility presumably arises from small numerical differences that occur when the equations are integrated over each cycle. It would be interesting to investigate the sensitivity and size of these differences for particles that come very close to each other.

The simulations show and the experiments confirm that the dynamical steady states and transition reported here require only that there be random displacements when particles approach too close. Whether this simple and versatile model can be adapted to understand self-organization in other driven non-equilibrium systems, and the nature of the minimal conditions to produce such a state, are intriguing topics for further research.

METHODS

Plastic (polymethylmethacrylate) transparent beads with a diameter of $230 \pm 20 \mu\text{m}$ (Diakron) are suspended in liquid consisting of a mixture of Triton-X100 (Sigma Aldrich), deionized water and zinc chloride (Fisher Scientific). Its composition is designed to match both the index of refraction and density of the particles^{25,26}. Fluorescent dye (Rhodamine 6G) is also added to the fluid to visualize the index-matched particles. The viscosity of the fluid is large ($\approx 3 \text{ Pa s}$, or about 3,000 times that of water) so that low-Re flow conditions are maintained at all times¹⁷. Particle volume fractions ranging from 0.2 to 0.4 were studied and all show similar behaviour. Shear experiments are performed using a Paar Physica MCR300 rheometer equipped with a customized Couette cell made of acrylic polymer so that both the Couette cylinders and the suspension have the same index of refraction. The system is thus completely transparent so that optical imaging can be used to follow particle motion. Particles are visualized by passing a sheet of laser light 200–300 μm thick through the cell (see the schematic diagram in Supplementary Information). For each measurement, the particle distribution is first randomized by shearing the system at a large strain amplitude $\gamma_0 = 5$ for 50 cycles. The sample is then sheared for 200 cycles at the desired strain amplitude γ_0 . During shearing, a laser sheet is directed through the gap of the Couette cell to reveal particles in the plane defined by the flow direction and the axis of the two cylinders. The distance of the imaging plane from the outer cylinder wall is about 0.5–1 mm or three to five particle diameters. Particle positions are recorded once per cycle with a camera and a frame grabber that are synchronized with the oscillating cylinder. About 500–1,000 particles are followed using this method and particle-tracking software²⁷. Fits to equation (1) for both simulation and experiments are realized by fixing δ and f_a^∞ and adjusting τ and f_a^0 . Satisfactory fits are obtained for values of $\delta = 0.15 \pm 0.05$ and 0.6 ± 0.05 for simulations and experiments respectively.

Received 16 September 2007; accepted 28 January 2008; published 16 March 2008.

References

- Hinrichsen, H. Non-equilibrium critical phenomena and phase transitions into absorbing states. *Adv. Phys.* **49**, 815–958 (2000).
- Mendes, J. F. F. Critical behaviour of models with infinitely many absorbing states. *Braz. J. Phys.* **30**, 105–112 (2000).
- Mollison, D. Spatial contact models for ecological and epidemic spread. *J. R. Stat. Soc. Ser. B* **39**, 283–326 (1977).
- Dickman, R. Nonequilibrium phase transitions in epidemics and sandpiles. *Physica A* **306**, 90–97 (2002).
- Ziff, R. M., Gulari, E. & Barshad, Y. Kinetic phase-transitions in an irreversible surface-reaction model. *Phys. Rev. Lett.* **56**, 2553–2556 (1986).
- Kohler, J. & Ben-Avraham, D. The dimer trimer model for heterogeneous catalysis. *J. Stat. Phys.* **65**, 839–848 (1991).
- Bouchaud, J. P. & Georges, A. Anomalous diffusion in disordered media—statistical mechanisms, models and physical applications. *Phys. Rep.-Rev. Sec. Phys. Lett.* **195**, 127–293 (1990).
- Havlin, S. & Ben-Avraham, D. Diffusion in disordered media. *Adv. Phys.* **51**, 187–292 (2002).
- Pomeau, Y. Front motion, metastability and subcritical bifurcations in hydrodynamics. *Physica D* **23**, 3–11 (1986).
- Dickman, R., Alava, M., Muñoz, M. A., Vespignani, A. & Zapperi, S. Critical behaviour of a one-dimensional fixed-energy stochastic sandpile. *Phys. Rev. E* **64**, 56104 (2001).
- Kinzel, W. *Percolation Structures and Processes* Vol. 5, 425 (Hilger, Bristol, 1983).
- Cardy, J. L. *Scaling and Renormalization in Statistical Physics* (Cambridge Univ. Press, New York, 1996).
- Broadbent, S. & Hammerley, J. Percolation processes. I. Crystals and mazes. *Proc. Camb. Phil. Soc.* **53**, 629 (1957).
- Janssen, H. K. On the non-equilibrium phase-transition in reaction–diffusion systems with an absorbing stationary state. *Z. Phys. B* **42**, 151–154 (1981).
- Grassberger, P. On phase-transitions in Schlogl 2nd model. *Z. Phys. B* **47**, 365–374 (1982).
- Grassberger, P. in *Nonlinearities in Complex Systems: Proc. 1995 Shimla Conf. on Complex Systems* (ed. Puri, S.) (Narosa, New Delhi, 1997).
- Pine, D. J., Gollub, J. P., Brady, J. F. & Leshansky, A. M. Chaos and threshold for irreversibility in sheared suspensions. *Nature* **438**, 997–1000 (2005).
- Eckstein, E. C., Bailey, D. G. & Shapiro, A. H. Self-diffusion of particles in shear-flow of a suspension. *J. Fluid Mech.* **79**, 191–208 (1977).
- Breedveld, V., van den Ende, D., Jongschaap, R. & Mellema, J. Shear-induced diffusion and rheology of noncolloidal suspensions: Time scales and particle displacements. *J. Chem. Phys.* **114**, 5923–5936 (2001).
- Drazer, G., Koplik, J., Khudid, B. & Acrivos, A. Microstructure and velocity fluctuations in sheared suspensions. *J. Fluid Mech.* **511**, 237–263 (2004).
- Dill, K. A. *et al.* Principles of protein-folding—a perspective from simple exact models. *Protein Sci.* **4**, 561–602 (1995).
- Vespignani, A., Dickman, R., Muñoz, M. A. & Zapperi, S. Driving, conservation, and absorbing states in sandpiles. *Phys. Rev. Lett.* **81**, 5676–5679 (1998).
- Rossi, M., Pastor-Satorras, R. & Vespignani, A. Universality class of absorbing phase transitions with a conserved field. *Phys. Rev. Lett.* **85**, 1803–1806 (2000).
- Sierou, A. & Brady, J. F. Rheology and microstructure in concentrated noncolloidal suspensions. *J. Rheol.* **46**, 1031–1056 (2002).
- Krishnan, G. P., Beimfohr, S. & Leighton, D. T. Shear-induced radial segregation in bidisperse suspensions. *J. Fluid Mech.* **321**, 371–393 (1996).
- Breedveld, V. *et al.* Measurement of the full shear-induced self-diffusion tensor of noncolloidal suspensions. *J. Chem. Phys.* **116**, 10529–10535 (2002).
- Crocker, J. C. & Grier, D. G. Methods of digital video microscopy for colloidal studies. *J. Colloid Interface Sci.* **179**, 298–310 (1996).

Acknowledgements

We thank J.-P. Bouchaud for suggesting the relevance of directed percolation and related models. We also benefited from discussions with E. Ben-Naim, S. Ramaswamy and G. I. Menon. This work was partially supported by National Science Foundation grants DMR 0604295 and DMR 0243001, and by a Lavoisier grant from the French government. Correspondence and requests for materials should be addressed to D.J.P. Supplementary Information accompanies this paper on www.nature.com/naturephysics.

Reprints and permission information is available online at <http://npg.nature.com/reprintsandpermissions/>